Anomalous temperature dependence of diode saturation currents in polycrystalline silicon thin-film solar cells on glass

J. Wong,[1,a)] J. L. Huang,[1] O. Kunz,[1] Z. Ouyang,[1] S. He,[1] P. I. Widenborg,[1] A. G. Aberle,[2] M. Keevers,[3] and M. A. Green[1]

[1]*Photovoltaics Centre of Excellence, The University of New South Wales, Sydney, New South Wales 2052, Australia*
[2]*Solar Energy Research Institute of Singapore (SERIS), National University of Singapore, 4 Engineering Drive 3, Singapore 117576, Singapore*
[3]*CSG Solar, 82 Bay Street, Botany, New South Wales 2019, Australia*

Temperature dependent Suns-V_{oc} measurements are performed on four types of polycrystalline silicon thin-film solar cells on glass substrates, all of which are made by solid phase crystallization/epitaxy of amorphous silicon from plasma enhanced chemical vapor deposition or e-beam evaporation. Under the two-diode model, the diode saturation currents corresponding to $n=1$ recombination processes for these polycrystalline silicon p-n junction cells follow an Arrhenius law with activation energies about $0.15-0.18$ eV lower than that of single-crystal silicon p-n diodes of 1.206 eV, regardless of whether the cells have an n- or p-type base. This discrepancy manifests itself unambiguously in a reduced temperature sensitivity of the open-circuit voltage in thin-film polycrystalline silicon solar cells compared to single-crystal silicon cells with similar voltages. The physical origin of the lowered activation energy is attributed to subgap levels acting either as minority carrier traps or shallow recombination centers. © 2009 American Institute of Physics.
[DOI: 10.1063/1.3131665]

I. INTRODUCTION

Polycrystalline silicon (poly-Si) fabricated on a glass has long been envisaged as a superior alternative to amorphous silicon (*a*-Si) for thin-film semiconductor devices, particularly solar cells[1] and thin-film transistors (TFTs) (Ref. 2) where the much larger mobility and diffusion length of poly-Si are important advantages for deriving high performance devices. Indeed, compared to *a*-Si, the structural, optical, and electrical properties of poly-Si are much closer to those of single-crystal silicon, which is often viewed as the ideal limit of poly-Si in the absence of structural defects. However, real poly-Si material is abundant with grain boundaries and extended intragrain defects, making it different from single-crystal silicon in a number of important ways. Optically, the absorptivity of poly-Si prepared by low pressure chemical vapour deposition (LPCVD),[3] sputtering,[4] and evaporation[5] has been found to be significantly higher than that of single-crystal silicon for photon energies below 1 up to 3 eV, with the extent of the enhancement dependent on the material preparation method. Electronically, there are consistent reports of band tails and a high density ($>10^{16}$/cm^3) of near midgap states in a variety of poly-Si films as determined by photothermal deflection spectroscopy,[3] admittance spectroscopy,[6] photoluminescence,[7] deep level transient spectroscopy,[8] electron paramagnetic resonance,[9] and field effect transistor analysis,[10–12] whereas these broad subgap states are absent in single-crystal silicon wafers. These anomalies profoundly influence the characteristics of poly-Si thin-film devices, such as the open-circuit voltage in solar cells and leakage current in TFTs.

In this paper we present another consistent feature in the diode characteristics of a variety of poly-Si on glass solar cells. Namely, the diode saturation currents of these poly-Si solar cells obey an Arrhenius law with significantly lower activation energies compared to typical single-crystal silicon counterparts. Such features have been reported earlier by Eggleston[5] for poly-Si material prepared by solid phase crystallization (SPC) of plasma enhanced chemical vapor deposition (PECVD) *a*-Si diodes. The aim of this paper is to examine a broader variety of poly-Si material, including those made from e-beam evaporated *a*-Si, as well as to deconvolve the various contributors to the unusual Arrhenius dependences. Since the diode saturation current is intimately related to the equilibrium concentration of minority carriers that undergo recombination in the device as well as the minority carrier lifetime, its activation energy sheds light on the mechanism of the dominant recombination process taking place in these poly-Si devices.

II. THEORY

A. Solar cell diode recombination current

The current-voltage relationship of poly-Si solar cells is well described by the two-diode model, which in the absence of resistive effects takes the form

$$J = J_L - J_{o1} \exp\left(\frac{qV}{kT}\right) - J_{o2} \exp\left(\frac{qV}{2kT}\right), \tag{1}$$

where J is the current density, J_L is the light induced current density, V is the terminal voltage and J_{o1}, J_{o2} are the diode saturation current densities for ideality factors of $n=1$ and $n=2$ recombination processes, respectively. Equation (1) holds true when $qV \gg kT$. Assuming predominance of base

a)Electronic mail: johnson.wong@unsw.edu.au.

diffusion current in J_{o1}, we may write it in the form

$$J_{o1} = \frac{qn_i^2}{n_o}\frac{D_p}{L_p}\frac{\sinh(W/L_p) + SL_p/D_p \cosh(W/L_p)}{\cosh(W/L_p) + SL_p/D_p \sinh(W/L_p)}, \qquad (2)$$

where q is the elementary charge, n_i is the intrinsic carrier concentration, n_o is the concentration of majority carriers (here assumed to be electrons) in the quasineutral region of the base, D_p and L_p are the diffusion coefficient and diffusion length of minority carriers (here assumed to be holes), respectively, and S is the cell rear surface recombination velocity. J_{o2} may arise at the junction depletion region or at extended defects, and it is instructive to write out its form for the former case,

$$J_{o2} = \sqrt{\frac{\pi}{2\tau_{no}\tau_{po}}}\frac{kTn_i}{E_o}, \qquad (3)$$

where τ_{no} and τ_{po} are the electron and hole capture lifetimes, respectively, and E_o is the magnitude of the electric field at the point in the depletion region where $\tau_{no}p = \tau_{po}n$. Generally, we may write the relationship between the diode saturation currents and temperature as

$$J_{on}(T) = J_{on}(T_o)\left(\frac{T}{T_o}\right)^{\gamma_n}\exp\left[-\frac{E_{act,n}}{k}\left(\frac{1}{T} - \frac{1}{T_o}\right)\right]. \qquad (4)$$

where T_o is a reference temperature, $n = 1, 2$ is the ideality factor, γ_n is the exponent of temperature, and $E_{act,n}$ is an activation energy reflecting the Arrhenius dependence of J_{on} on the temperature T.

B. The case of single-crystal silicon (recombination via deep levels)

In an ideal single-crystal silicon solar cell whose recombination rate is dominated by deep levels, the minority carrier lifetime under low injection conditions is approximately given by $\tau_{SRH}^{LLI} = (N_t v_{th}\sigma)^{-1}$, where N_t is the defect concentration, v_{th} is the minority carrier thermal velocity, and σ is the capture cross section for minority carriers. If σ can be regarded as temperature independent, then overall τ_{SRH}^{LLI}, and thus $L_P = (D_P\tau_{SRH}^{LLI})^{1/2}$, are only slightly temperature dependent via the weak power law T dependences of v_{th} and D_p. This leaves n_i in Eqs. (2) and (3) as the only term with Arrhenius dependence on temperature, as it is given by

$$n_i^2 = N_c N_v \exp\left(-\frac{E_g(T)}{kT}\right), \qquad (5)$$

where N_c and N_v are the conduction and valence band effective density of states, respectively, and $E_g(T)$ is the band gap. Substituting Eq. (5) into Eqs. (2) and (3) and then comparing with Eq. (4), one finds $E_{act,1} = 2E_{act,2} = E_{go}$, where $E_{go} = E_g(T) - T(\partial E_g/\partial T)$, the band gap linearly extrapolated to 0 K from the temperature of interest. For single-crystal silicon $E_{go} = 1.206$ eV.[13]

C. The case of polycrystalline silicon

In semiconductors with subgap states that are in the vicinity of the majority carrier Fermi level E_F, terms other than n_i in Eq. (2) may exhibit Arrhenius laws. If the subgap states
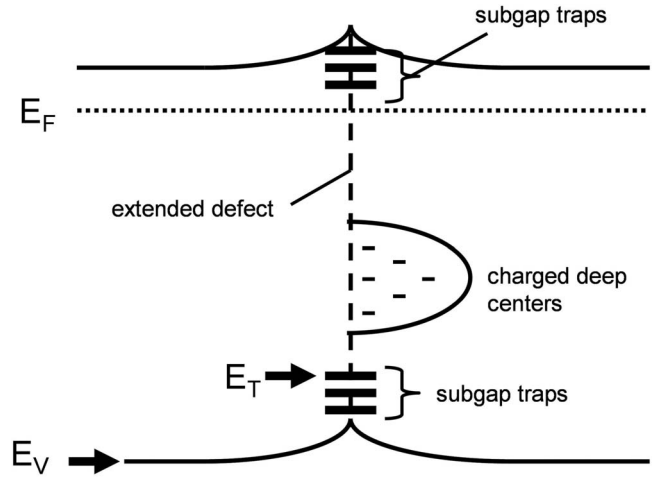

FIG. 1. Illustration of subgap traps at characteristic energy level E_T compared to the band edge level E_V. Here the traps occur at an extended defect where the band bending further raises E_T. Minority carriers trapped at E_T may participate in the dominant recombination process.

are recombination centers, carrier emission rates may be comparable to or greater than capture rates, causing the minority carrier lifetime to become temperature dependent.[14–16] Similarly, if these states are acting as minority carrier traps, via which carriers recombine at a deeper level, then the minority carrier lifetime will also have Arrhenius dependence through the ratio of minority carriers in trapped and extended states.[17] Finally, if the subgap states exist at extended defects, local extrema of a fluctuating band edge due to stress[18] or band bending due to trapped charges can further increase this ratio by attracting minority carriers. Each of these case results in $E_{act,1} < E_{go}$. The general picture is depicted in Fig. 1. Here the relevant subgap level is denoted by E_T and the bulk band edge level is denoted by E_V.

Another effect of subgap states lying in the vicinity of E_F is their ability to act as counterdopants by trapping majority carriers. As the temperature rises, E_F moves deeper into the bandgap, causing the majority carrier occupancy in traps to decrease and the free carrier concentration n_o to increase. This will also contribute to the inequality $E_{act,1} < E_{go}$.

III. EXPERIMENTAL PROCEDURES

We have examined four types of poly-Si on planar glass solar cells: (1) a glass|SiN|n^+pp^+ diode formed by SPC from an a-Si precursor deposited by PECVD, dubbed PLASMA;[19] (2) a glass|SiN|p^+nn^+ diode formed by solid phase epitaxy from an a-Si precursor deposited by e-beam evaporation on a thin ($\sim$50 nm), large grain poly-Si seed layer, dubbed ALICE;[20] (3) a glass|SiN|n^+pp^+ diode formed by SPC from an a-Si precursor deposited by e-beam evaporation, dubbed EVA1;[21] and (4) a second diode fabricated in the same way as EVA1, but with a glass|np^+ structure, which we call EVA2. The special layer sequence of EVA2 enabled one to etch off the top p^+ emitter layer in order to measure optical transmission through the n-type base material. The cells are deposited on borosilicate or boroaluminosilicate glass coated with $\sim$60 nm silicon nitride (SiN) antireflection layer, with
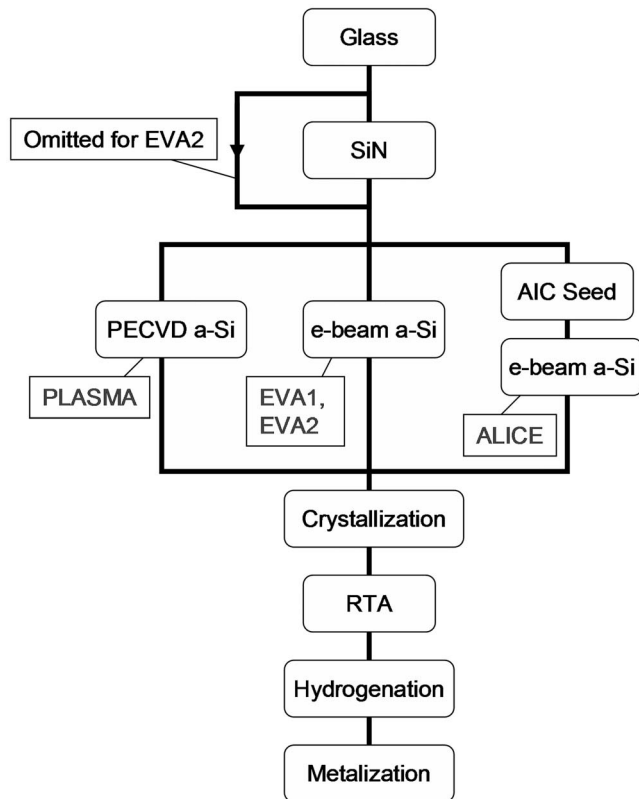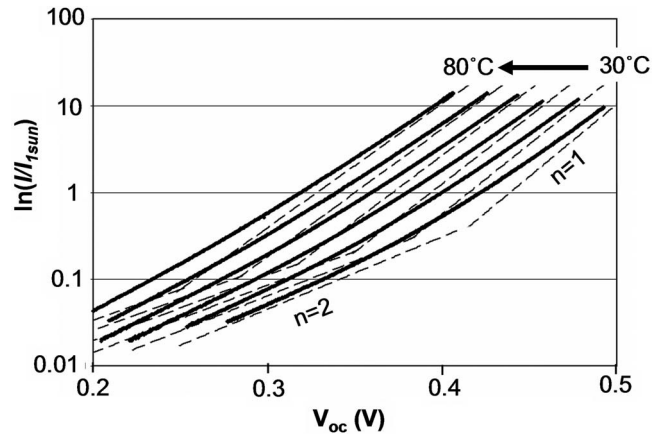
FIG. 2. Process sequence of the poly-Si solar cells.

FIG. 3. Superposition of Suns-V_{oc} curves of EVA2 from 30 to 80 °C. For clarity, only six curves corresponding to 10 °C increments are shown. The dashed lines represent the fits to the $n=1$ and $n=2$ recombination currents.

the exception of EVA2 where the SiN layer is omitted. The lightly doped base layers in all the cells have thickness from 2 to 3 μm, with a dopant density in the 10^{16}–2×10^{17} cm^{-3} range. After crystallization, the poly-Si diodes received a rapid thermal anneal (RTA) at temperatures of ~900 °C for ~4 min. Finally the cells underwent a hydrogen plasma treatment at plateau temperatures in the range of 600–650 °C for 15–20 min in a LPCVD system with an inductively coupled remote plasma source. Both postdeposition treatments (RTA and hydrogenation) are essential processes for achieving appreciable performance of the discussed poly-Si solar cells.[22,23] PLASMA, EVA1, and EVA2 have grain size of about 1 μm and ALICE has a grain size of about 10 μm. Figure 2 outlines the process sequence of the four solar cells. After fabrication, smaller cells (~1 cm^2) are defined on the films by isolation etching.

We used the Suns-V_{oc} method[24] to extract J_{o1} and J_{o2} of the solar cells at different temperatures. The Suns-V_{oc} instrumentation used for this work has been detailed elsewhere.[25] Briefly, a decaying light pulse with a full width half maximum of about 2 ms from a xenon flash lamp induces a quasisteady state photovoltage V_{oc} across the p-n junction in open-circuit condition. The light intensity is monitored by a single-crystal silicon reference cell and plotted against V_{oc}. Temperature dependent measurements are performed by enclosing the sample stage and electrical probes in a thermally insulated chamber with an acrylic glass window. The chamber air is heated by a bank of resistors and its temperature is monitored by a PT100 platinum resistance thermocouple placed next to the sample. The chamber and contents are allowed to cool unaided from peak temperature (80–90 °C)

at a slow rate (<0.5 °C/min) to room temperature, and one Suns-V_{oc} curve is captured for every incremental 1 °C drop. The same sample chamber is used to measure the external quantum efficiency (EQE) at different temperatures in order to estimate J_L in Eq. (1).

Although Suns-V_{oc} circumvents the problem present in dark J-V measurements, where the voltage can be skewed by series resistance effects, it is however susceptible to contact photovoltages arising at high light intensities.[26] Thus it is important to ensure that the metal-semiconductor contacts for probing terminal voltage are Ohmic. We accomplish this by evaporating an Al grid on the highly doped air-side poly-Si layer, following a piranha clean and HF dip, and additionally baking the contact in an N$_2$ ambient at 200–250 °C for 30 min if the air-side layer is p^+ type, in order to lower the Al–Si contact barrier.[27] The glass-side poly-Si layer is exposed by timed etching, cleaned, and then contacted by either evaporated Al (EVA1 and ALICE) or a GaAl alloy paint (EVA2 and PLASMA).

For optical measurements, we etched off the p^+ emitter of one of the cells on EVA2 to obtain a uniform film composed of n-type base material. Transmission through the sample into an integrating sphere is measured from 300 to 1800 nm using a Varian CARY 5G spectrophotometer. Hall measurement is performed on an adjacent area of the sample in order to measure the majority carrier concentration.

IV. RESULTS AND DISCUSSION

A. The relation of light induced current and diode saturation currents with temperature

For the point of illustration, Fig. 3 shows a series of Suns-V_{oc} curves obtained from EVA2 over the scanned temperature range. We may rewrite Eq. (1) in a way that is more relevant to the Suns-V_{oc} conditions,

$$I = \left[\frac{J_{o1}}{(J_L/I)}\right]\exp\left(\frac{qV_{oc}}{kT}\right) + \left[\frac{J_{o2}}{(J_L/I)}\right]\exp\left(\frac{qV_{oc}}{2kT}\right), \qquad (6)$$

where I is the illumination intensity. The aggregate terms in the square brackets are the coefficients to the diode current
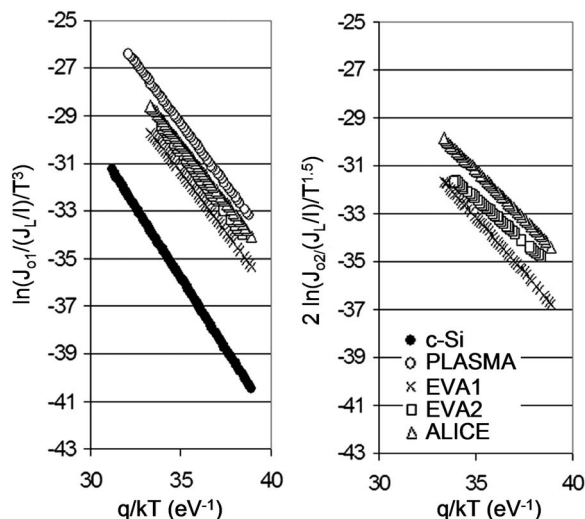
FIG. 4. Arrhenius plots of $J_{o1}/(J_L/I)$ and $J_{o2}/(J_L/I)$ of the poly-Si solar cells. $J_{o1}/(J_L/I)$ for a single-crystal silicon wafer solar cell is also shown for comparison.

FIG. 5. Short-circuit current density (J_{sc}) of the solar cells under the xenon lamp spectrum as a function of temperature.

terms which can be extracted by plotting I versus V_{oc}. Clearly, on the semilog plot, the curves are approximately piecewise linear, with the steeper slope region at higher Suns being $n=1$ dominated and the flatter slope region at low Suns being $n=2$ dominated. Extracting $J_{o1}/(J_L/I)$ and $J_{o2}/(J_L/I)$ at each temperature enables one to construct the Arrhenius plots for each poly-Si solar cell, as shown in Fig. 4. $J_{o2}/(J_L/I)$ for PLASMA is not shown because the $n=2$ region of this cell is too low to be accurately fitted from the Suns-V_{oc} plots in the measured light intensity range. For comparison, we also display the $J_{o1}/(J_L/I)$ for a boron doped (7.5×10^{16} cm^{-3}) single-crystal silicon wafer solar cell. Considering the various power law dependencies of the terms in J_{o1} and J_{o2} on temperature, γ_1 should lie between 2.8 and 3.5 and γ_2 should be about 1.5. For simplicity, we have chosen $\gamma_1=3$ and $\gamma_2=1.5$ for all the solar cells studied. One readily sees that, for the Arrhenius plots of $J_{o1}/(J_L/I)$, there is a remarkable consistency in the slopes of the lines belonging to poly-Si cells, which are distinctly different from those of the single-crystal silicon cell. This reflects that the activation energy associated with the quotient $J_{o1}/(J_L/I)$ is lower in the poly-Si cells compared to the single-crystal silicon cell.

In order to discern the temperature characteristics of J_{on} and (J_L/I) individually, we show in Fig. 5 the Arrhenius plots of short-circuit current density (J_{sc}) of the solar cells under the xenon lamp spectrum as a function of temperature, as calculated from EQE measurements. EVA2 is omitted because its simplified structure makes it difficult to extract current. Here we assume that $J_L=J_{sc}$, which is, in general, a sound approximation. Not surprisingly, J_L for the single-crystal silicon solar cell does not vary significantly with temperature, changing by about 620 ppm/°C which is somewhat larger than the theoretical value of 167 ppm/°C if one expects only the effect of band gap narrowing with temperature.[28] For poly-Si cells, both EVA1 and ALICE experience pronounced rise in J_L as temperature increases—with temperature sensitivites of 5400 and 4700 ppm/°C—too large to be explained by the band gap
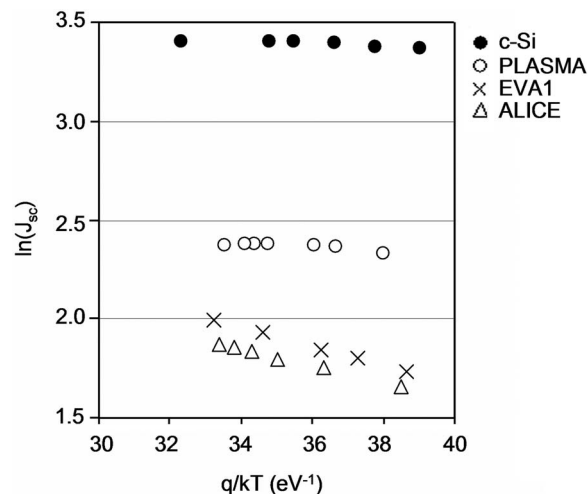
narrowing effect. Meanwhile, J_L for PLASMA does not change significantly with temperature. Curve fitting to EQE data shows that among all the solar cells discussed, only the PLASMA has a diffusion length that is comparable or longer than the base thickness in the temperature range measured, the rest having diffusion lengths which are at most half the base thickness. Clearly, the single-crystal silicon cell has a diffusion length which is insensitive to temperature, while the poly-Si cells have diffusion lengths which increase as the cells get hotter, causing J_L to rise with temperature when the diffusion length is shorter than the base thickness. As it is intuitively clear, a temperature dependent diffusion length affects not only (J_L/I) but also J_{o1} through the L_p term in the denominator of Eq. (2). In the following, we shall show that E_{act1} (the activation energy of J_{o1}) is indeed deviated from E_{go} in a consistent manner.

Table I summarizes the four poly-Si and single-crystal silicon cell types and the activation energies associated with $J_{o1}/(J_L/I)$, $J_{o2}/(J_L/I)$, (J_L/I), and E_{act1}, E_{act2} which are derived from the first three quantities. We obtain $E_{act1}=1.197$ eV for the single-crystal silicon cell, which is in good agreement with the value of $E_{go}=1.206$ eV quoted in literature.[13] On the other hand, the E_{act1} values of the poly-Si cells are significantly lower, in the range of 1.026–1.053 eV—i.e., lower than E_{go} by about 0.15–0.18 eV, and the $2E_{act2}$ values are lower still in the range of 0.894–1.015 eV. These activation energies for poly-Si are in close agreement with Eggleston's reported values for poly-Si solar cells made by SPC of PECVD deposited a-Si diodes.[5] The larger scatter in $2E_{act2}$ is likely due to fewer Suns-V_{oc} data points for fitting in the $n=2$ regime.

B. Physical origin of the activation energies

The unusual temperature sensitivities in both (J_L/I) and J_{o1} are consistent indicators that the bulk minority carrier lifetime—playing a role in both light induced current and diode saturation currents—follows an Arrhenius temperature dependence. As discussed in Sec. II, this can stem from shallow subgap states acting as either fast minority carrier traps

TABLE I. Base layer parameters and E_{act1} and $2E_{act2}$ values of the poly-Si solar cells. The extracted E_{act1} of the single-crystal silicon solar cell is also shown for comparison.

| Cell | Type | Base doping density (cm^{-3}) | Activation energy of | | | E_{act1} (eV) | $2E_{act2}$ (eV) | $V_{oc} - T\frac{\partial V_{oc}}{\partial T}$ (V) |
			$\frac{J_L/I}{}$ (eV)	$\frac{J_{o1}}{(J_L/I)}$ (eV)	$\frac{J_{o2}}{(J_L/I)}$ (eV)			
Single-crystal silicon	p	7.5×10^{16}	0.006	1.191	$\cdots$	1.197[a]	$\cdots$	1.272[b]
PLASMA	p	1.5×10^{16}	0.008	1.021	$\cdots$	1.029	$\cdots$	1.086
EVA1	p	1.7×10^{17}	0.049	1.004	0.459	1.053	1.015	1.071
EVA2	n	1.4×10^{17}	$\cdots$	1.012	0.352	$\cdots$	$\cdots$	1.029
ALICE	n	4.7×10^{16}	0.042	0.984	0.405	1.026	0.894	1.011

[a]Theoretical value is $E_{go} = 1.206$ eV (Ref. 13).
[b]Theoretical value is about 1.270 eV (See Sec. IV C).

or recombination centres. The latter effect has been reported in certain single-crystal silicon wafers intentionally contaminated with metal impurities,[29–32] as well as epitaxial silicon thin-film solar cells prepared by ion-assisted deposition.[15] The energy level of the relevant subgap states relative to the closest band edge, $|E_C - E_T|$ or $|E_V - E_T|$, would then be a contributor to $E_{go} - E_{act1}$ with a factor that is dependent on the form of Eq. (2). The possibility that the dominant recombination process involves such shallow subgap states is highly plausible since it is well known that radiative recombination in poly-Si occurs in this way. Photoluminescence[7] and cathodoluminescence[33,34] signals at $0.8-1.0$ eV are widely reported in various poly-Si materials, while band-to-band luminescence is not observed.

In addition, dopant compensation by shallow majority carrier traps affects J_{o1} through the term n_o in Eq. (2), and its temperature dependence will also make a contribution to E_{act1}. Hall measurements on the base layer of EVA2 shows that the majority carrier concentration indeed raises with temperature, but on an Arrhenius plot, it leads to an activation energy of only $0.02-0.03$ eV, which is a relatively minor contribution.

There have been reports that poly-Si material, made by LPCVD (Ref. 3) and sputtering,[4] have smaller band gap compared to single-crystal silicon. While a small band gap may explain the unusually low E_{act1}, it cannot account for the temperature sensitivity of (J_L/I). Further, we shall show now that the optical band gap of the poly-Si material reported in this work is sufficiently close to that of single-crystal silicon that it cannot account for the large difference in $E_{go} - E_{act1}$. Figure 6 shows the optical transmission spectrum of the EVA2 n-type base layer. The filled circles are a fit of transmission through this glass$|n$ structure assuming single-crystal silicon optical properties for the n-layer, allowing for nonuniformity in the film thickness whose treatment has been described elsewhere.[4] The excellent fit for wavelengths above 800 nm shows that the absorptivities of the EVA2 poly-Si base layer and single-crystal silicon material are similar near the band edge—within a factor of 2 of each other in the range of $800-1000$ nm ($1.2-1.55$ eV), according to sensitivity analysis and not differing by more than 100 cm^{-1} for wavelengths greater than 1000 nm. This is in contrast to the previously reported poly-Si material whose absorptivity differs from single-crystal silicon by three to six times at 1000 nm and is greater by more than 100 cm^{-1} even at 1200 nm.[3,4] Considering that these reports quote values for the poly-Si band gap of about 1 eV, it is reasonable to conclude that the band gap of EVA2 base material is significantly higher than 1 eV—not possibly differing from that of single-crystal silicon by more than 0.1 eV. Therefore the difference of $E_{go} - E_{act1} = 0.15 - 0.18$ eV cannot be adequately explained by a smaller bandgap in poly-Si compared to single-crystal silicon if a significant difference exists at all.

C. Implications on device characteristics

Aside from the J_{sc} being sensitive to temperature, the temperature dependence of the poly-Si solar cell's V_{oc} and ideality factor n are also somewhat different from those of the single-crystal silicon solar cell as a result of E_{act1}, E_{act2}, and the activation energy of (J_{sc}/I).[35] Substituting Eq. (4) into Eq. (6), one obtains
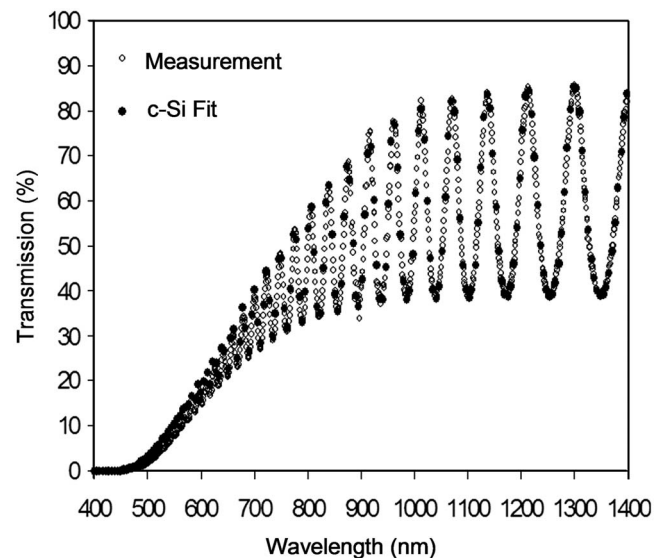

FIG. 6. Optical transmission spectrum of the EVA2 n-type base layer. The filled circles are a fit of transmission through this glass$|n$ structure assuming single-crystal silicon optical properties for the n-layer. Fitted n-layer thickness is 2410 nm with 47 nm thickness variation.
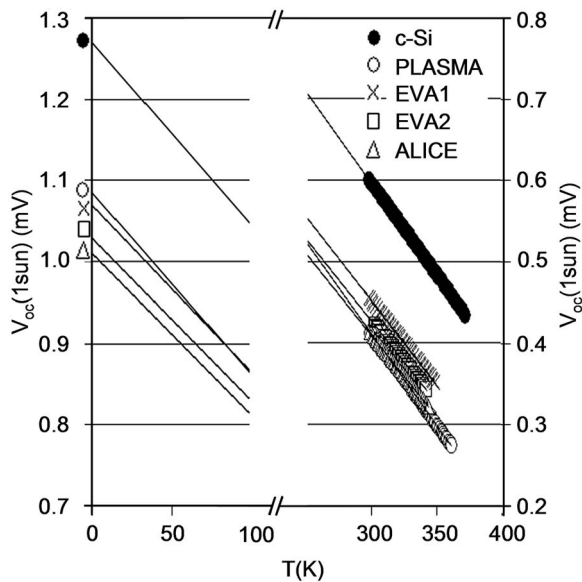
FIG. 7. V_{oc}(1 sun) of the poly-Si solar cells as a function of temperature compared to that of a single-crystal silicon solar cell. The straight lines extending from the data points are extrapolations.

$$I = \frac{1}{(J_L/I)} \cdot \left(J_{o1}(T_o)\exp\left(\frac{E_{act1}}{kT_o}\right)\left(\frac{T}{T_o}\right)^{\gamma_1} \right.$$
$$\times\exp\left(-\frac{E_{act1} - qV_{oc}}{kT}\right) + J_{o2}(T_o)\exp\left(\frac{2E_{act2}}{2kT_o}\right)\left(\frac{T}{T_o}\right)^{\gamma_2}$$
$$\left. \times\exp\left(-\frac{2E_{act2} - qV_{oc}}{2kT}\right) \right). \qquad (7)$$

From Eq. (7), it can be shown that the temperature sensitivity of the V_{oc} at one Sun illumination $[V_{oc}(1 \text{ sun})]$ obeys

$$2E_{act2} + 2\gamma_2 kT - kT^2\frac{\partial \ln J_L}{\partial T}$$
$$\leq qV_{oc}(1 \text{ sun}) - T\frac{\partial qV_{oc}(1 \text{ sun})}{\partial T}$$
$$\leq E_{act1} + \gamma_1 kT - kT^2\frac{\partial \ln J_L}{\partial T} \qquad (8)$$

such that the low values of E_{act1} and E_{act2} in poly-Si cells contribute to decrease the V_{oc}(1 sun) sensitivity compared to single-crystal silicon cells with the same open-circuit voltages. Figure 7 plots V_{oc}(1 sun) against temperature for the poly-Si cells and the single-crystal silicon cell. Indeed, for the single-crystal silicon solar cell the $T=0$ intercept takes on a value of 1.272 V, which corresponds closely to the predicted value of 1.270 V according to Eq. (8) assuming that $E_{act1} = 2E_{act2} = E_{go}$ and $\partial(\ln J_L)/\partial T = 0$. For the poly-Si solar cells, the intercepts are comparatively lower at 1.00–1.10 V, and they also fall within the respective upper and lower bounds given by Eq. (8).

Referring to the Suns-V_{oc} curves in Fig. 3, one sees that the point of transition from $n=1$ to $n=2$ diode current moves toward lower light intensity as the temperature increases. This causes the local ideality factor at the maximum power point to decrease as temperature increases. The physical ori-

gin of this effect can be explained as follows. From Eq. (7) one can deduce that the $n=1$ to $n=2$ transition occurs when

$$\ln(I)|_{\text{transition}} = \frac{E_{act1} - 2E_{act2}}{kT} - \frac{E_{act1} - 2E_{act2}}{kT_o}$$
$$+ \ln\left[\frac{2J_{o2}(T_o)^2}{J_{o1}(T_o)}\frac{1}{(J_L/I)}\left(\frac{T}{T_o}\right)^{2\gamma2-\gamma1}\right]. \qquad (9)$$

There are two previously discussed factors that causes $\ln(I)|_{\text{transition}}$ to move downward with temperature according to Eq. (9): (i) (J_L/I) increases with temperature and (ii) $E_{act1} > 2E_{act2}$. The former effect has been attributed to a temperature dependent lifetime, as discussed in Sec. VI B, while the physical origin of the latter inequality remains unclear at this stage.

V. CONCLUSIONS

The consistency of $E_{go} - E_{act1}$ (0.15–0.18 eV) across the several types of poly-Si thin-film solar cells on glass studied, including both n-type and p-type base layers prepared by different methods, points toward a fundamental difference in the carrier recombination pathway between thin-film poly-Si on glass and bulk single-crystal silicon materials. Coupled with the fact that the light generated current J_L raises significantly with temperature in the poly-Si cells whose diffusion lengths are shorter than the base thickness, there are likely relatively shallow subgap states at some energy $|E_{ext} - E_T|$ from the closest band edge are acting either as fast minority carrier traps or recombination centres. This is further supported by the observations of luminescence at energies below the silicon band gap in poly-Si thin-film materials, which is a direct evidence of carriers trapped in subgap states undergoing radiative recombination. Other factors that influence $E_{go} - E_{act1}$, including a narrowed band gap compared to single-crystal silicon and temperature dependent dopant compensation, may also make small contributions and they require more accurate measurements in order to determine $|E_{ext} - E_T|$. From a technological point of view, the validation and further understanding of the recombination mechanism, specifically how it relates to structural and compositional defects in poly-Si thin films, is of paramount importance for improving the efficiency of poly-Si thin-film solar cells.

[1] R. B. Bergmann, Appl. Phys. A: Mater. Sci. Process. **69**, 187 (1999).
[2] S. D. Brotherton, Semicond. Sci. Technol. **10**, 721 (1995).
[3] W. B. Jackson, N. M. Johnson, and D. K. Biegelsen, Appl. Phys. Lett. **43**, 195 (1983).
[4] B. S. Richards, A. Lambertz, and A. B. Sproul, Thin Solid Films **460**, 247 (2004).

[5]B. Eggleston, Undergraduate thesis, University of New South Wales, 2005.

[6]J. Werner and M. Peisl, Phys. Rev. B **31**, 6881 (1985).

[7]A. U. Savchouk, S. Ostapenko, G. Nowak, J. Lagowski, and L. Jastrzebski, Appl. Phys. Lett. **67**, 82 (1995).

[8]J. R. Ayres, J. Appl. Phys. **74**, 1787 (1993).

[9]D. Ballutaud, M. Aucouturier, and F. Babonneau, Appl. Phys. Lett. **49**, 1620 (1986).

[10]C. A. Dimitriadis, D. H. Tassis, N. A. Economou, and A. J. Lowe, J. Appl. Phys. **74**, 2919 (1993).

[11]B. A. Khan and R. Pandya, IEEE Trans. Electron Devices **37**, 1727 (1990).

[12]T. J. King, M. G. Hack, and I. W. Wu, J. Appl. Phys. **75**, 908 (1994).

[13]S. M. Sze, *Physics of Semiconductor Devices* (Wiley, New York, 1969), p. 24.

[14]T. A. Wagner and U. Rau, Appl. Phys. Lett. **82**, 2637 (2003).

[15]S. Rein, T. Rehrl, W. Warta, and S. W. Glunz, J. Appl. Phys. **91**, 2059 (2002).

[16]W. Shockley and W. T. Read, Phys. Rev. **87**, 835 (1952).

[17]J. A. del Alamo and R. M. Swanson, Jpn. J. Appl. Phys., Part 1 **26**, 1860 (1987).

[18]M. A. Green (private communication).

[19]P. I. Widenborg and A. G. Aberle, Adv. OptoElectron. **2007**, 24584 (2007).

[20]P. I. Widenborg, A. Straub, and A. G. Aberle, J. Cryst. Growth **276**, 19 (2005).

[21]O. Kunz, J. Wong, J. Janssens, J. Bauer, O. Breitenstein, and A. G. Aberle, Prog. Photovoltaics **17**, 35 (2009).

[22]M. L. Terry, D. Inns, and A. G. Aberle, Adv. OptoElectron. **2007**, 83657 (2007).

[23]M. J. Keevers, A. Turner, U. Schubert, P. A. Basore, and M. A. Green, Proceedings of the 20th European Photovoltaic Solar Energy Conference, Barcelona, 2005 (unpublished), p. 1305.

[24]R. A. Sinton and A. Cuevas, Proceedings of the 16th European PV Solar Energy Conference, Glasgow (2000) (unpublished), pp. 1152–1155.

[25]O. Kunz, MS thesis, Carl von Ossietzky Universität, University of New South Wales, 2005.

[26]S. W. Glunz, J. Nekarda, H. Mackel, and A. Cuevas, Proceedings of the 22nd European Photovoltaic Solar energy Conference and Exhibition, Milano, 2007 (unpublished), pp. 3–7.

[27]H. C. Card, IEEE Trans. Electron Devices **23**, 538 (1976).

[28]M. A. Green, Prog. Photovoltaics **11**, 333 (2003).

[29]A. Kaniava, A. L. P. Rotondaro, J. Vanhellemont, U. Menczigar, and E. Gaubas, Appl. Phys. Lett. **67**, 3930 (1995).

[30]F. Shimura, T. Okui, and T. Kusama, J. Appl. Phys. **67**, 7168 (1990).

[31]Y. Kirino, A. Buczkowski, Z. J. Radzimski, G. A. Rozgonyi, and F. Shimura, Appl. Phys. Lett. **57**, 2832 (1990).

[32]D. Macdonald, A. Cuevas, S. Rein, P. Lichtner, and S. W. Glunz, Proceedings of the Third World Conference on Photovoltaic Energy Conversion, 2003 (unpublished), Vol. 1, pp. 87–90.

[33]F. Liu, M. J. Romero, K. M. Jones, A. G. Norman, M. M. Al-Jassim, D. Inns, and A. G. Aberle, Thin Solid Films **516**, 6409 (2008).

[34]D. Van Gestel, M. J. Romero, I. Gordon, L. Carnel, J. D'Haen, G. Beaucarne, M. Al-Jassim, and J. Poortmans, Appl. Phys. Lett. **90**, 092103 (2007).

[35]J. Huang, J. Wong, M. A. Green, and M. Keevers, Proceedings of the 18th International Photovoltaic Science and Engineering Conference and Exhibition (unpublished).